Molecular Theory of Lipid-Protein Interaction and the L_α-H_{II} Transition

Sylvio May and Avinoam Ben-Shaul

Department of Physical Chemistry and the Fritz Haber Research Center, The Hebrew University of Jerusalem, Jerusalem 91904, Israel

ABSTRACT   We present a molecular-level theory for lipid-protein interaction and apply it to the study of lipid-mediated interactions between proteins and the protein-induced transition from the planar bilayer (L_α) to the inverse-hexagonal (H_{II}) phase. The proteins are treated as rigid, membrane-spanning, hydrophobic inclusions of different size and shape, e.g., "cylinder-like," "barrel-like," or "vase-like." We assume strong hydrophobic coupling between the protein and its neighbor lipids. This means that, if necessary, the flexible lipid chains surrounding the protein will stretch, compress, and/or tilt to bridge the hydrophobic thickness mismatch between the protein and the unperturbed bilayer. The system free energy is expressed as an integral over local molecular contributions, the latter accounting for interheadgroup repulsion, hydrocarbon-water surface energy, and chain stretching-tilting effects. We show that the molecular interaction constants are intimately related to familiar elastic (continuum) characteristics of the membrane, such as the bending rigidity and spontaneous curvature, as well as to the less familiar tilt modulus. The equilibrium configuration of the membrane is determined by minimizing the free energy functional, subject to boundary conditions dictated by the size, shape, and spatial distribution of inclusions. A similar procedure is used to calculate the free energy and structure of peptide-free and peptide-rich hexagonal phases. Two degrees of freedom are involved in the variational minimization procedure: the local length and local tilt angle of the lipid chains. The inclusion of chain tilt is particularly important for studying noncylindrical (for instance, barrel-like) inclusions and analyzing the structure of the H_{II} lipid phase; e.g., we find that chain tilt relaxation implies strong faceting of the lipid monolayers in the hexagonal phase. Consistent with experiment, we find that only short peptides (large negative mismatch) can induce the $L_\alpha \rightarrow H_{II}$ transition. At the transition, a peptide-poor L_α phase coexists with a peptide-rich H_{II} phase.

INTRODUCTION

Proteins interact with membranes in different ways. They can adsorb to the lipid headgroup region, partially penetrate the hydrophobic core, or fully span the bilayer membrane. In most cases the protein interacts with both the hydrophilic headgroup region and the hydrophobic interior of the membrane; yet, at least approximately, these interactions are separable. The outcome of the interaction depends on the structure and chemical composition of both the protein and the lipid membrane. For example, integral hydrophobic proteins embedded in multicomponent ("mixed") membranes tend to surround themselves with lipids of matching chain length, thus inducing local demixing of the lipid components. At high enough protein concentration, this preferential "wetting" may lead to global phase separation. Similarly, electrostatically adsorbed charged proteins can induce the formation of (oppositely) charged lipid domains.

Our interest in this paper focuses on integral, membrane-spanning proteins. More specifically, our goal is to analyze the role of protein size and shape in lipid-protein interaction, with special emphasis on lipid-mediated protein-protein interactions and the protein-mediated transition from the planar bilayer (L_α) to the inverse hexagonal (H_{II}) lipid phase. To study these phenomena, we shall treat the protein as a rigid hydrophobic inclusion, thus ignoring specific chemical and steric interactions between the protein and the surrounding lipids. Furthermore, although the present theory can be extended to treat mixed lipid membranes, in this paper we shall only consider single-component ("pure") bilayers. The constituent lipids will be characterized by their hydrophobic chain length, the strength of the repulsive interaction between their polar headgroups, and the hydrocarbon-water surface energy. These characteristics dictate the structural and elastic properties of the lipid layer, namely, the equilibrium area and ("spontaneous") curvature, as well as the bending and area-compressibility moduli of the membrane. Another, less familiar elastic constant that can be expressed in terms of the molecular force constants appearing in our model is the tilt modulus of the lipid chains.

The key factor for stable integration of proteins into membranes is strong hydrophobic coupling or, in other words, maximum overlap between the hydrophobic regions of the protein and the membrane, so as to minimize the exposure of these regions to the aqueous solvent. Interestingly, the match between the hydrophobic regions of the protein and the (protein-free) host membranes need not be an optimal one. Indeed, for some systems it is known that a certain degree of *hydrophobic mismatch,* i.e., a difference between the hydrophobic thickness of the protein and that of the ("unperturbed") bilayer, can still be accommodated by the membrane (Killian, 1998; Lewis and Engelmann, 1983). This fact has initiated considerable experimental work on how a protein (or peptide) and a bilayer membrane would respond to a given hydrophobic mismatch. For example, it was shown that hydrophobic mismatch can drive lateral

reorganization and aggregation of proteins in membranes (Ryba and Marsh, 1992), affect the lipid melting transition (Piknova et al., 1993), and lead to molecular lipid sorting in mixed membranes (Dumas et al., 1997). Other possible mechanisms involve a change in the peptide transmembrane orientation (e.g., helix tilt; Ren et al., 1997) or conformational modifications of the protein that may be accompanied by a change in protein activity (Killian, 1998). Conversely, proteins can induce morphological changes in the embedding lipid environment. More specifically, it was recently shown that some artificial, hydrophobic α-helical peptides (Killian et al., 1996; Morein et al., 1997) as well as gramicidin A (Killian, 1992; Killian and deKruijff, 1988) are able to induce a morphological change of a bilayer in its fluid, L_α, phase into a nonlamellar structure, such as the inverse hexagonal, H_{II}, phase.

The peptide-mediated $L_\alpha \rightarrow H_{II}$ transition is remarkable because the lipids used in the above experiments are phosphatidylcholines, which, in the absence of peptide, self-assemble into planar bilayers. It was found that the transition from the lamellar to the inverse hexagonal (or an isotropic) phase depends strongly on the degree of hydrophobic mismatch and the initial peptide concentration. More explicitly, the appearance of the $L_\alpha \rightarrow H_{II}$ transition requires a large *negative* hydrophobic mismatch; that is, the hydrophobic peptide span must be considerably shorter than the equilibrium hydrophobic thickness of the bilayer. In this case, the maximum solubility of the peptide in the bilayer corresponds to a molar peptide/lipid ratio of roughly 1/30. The peptide concentration in the ensuing H_{II} phase is highly enriched, corresponding to a peptide/lipid ratio of $\sim 1/6$. Based on qualitative packing considerations, it was suggested that the peptides in the H_{II} phase are concentrated in the regions between neighboring tubules of the hexagonal lattice, spanning the entire hydrophobic thickness in these regions (Killian et al., 1996; Morein et al., 1997; Killian, 1992). In Fig. 1 we show the structure of the peptide containing L_α and H_{II} phases, the latter according to the model proposed by Killian. It should be noted that all of the peptides known so far to induce the $L_\alpha \rightarrow H_{II}$ transition are uncharged, their N- and C-termini are blocked, and they contain tryptophan residues that are localized near the hydrocarbon-water interface of the membrane. It has been suggested that these interface-anchored tryptophans prevent peptide aggregation in the membrane.
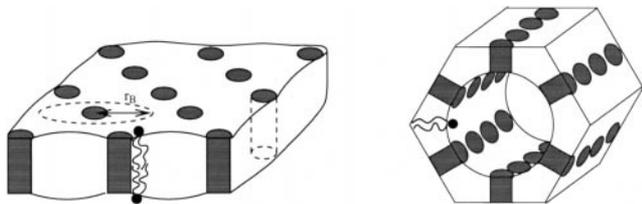
FIGURE 1   Structural models of the lipid-peptide matrix: the bilayer, L_α, phase (*left*) and the inverse hexagonal, H_{II}, phase (*right*), the latter as suggested by Killian et al. (1996).

We have two major objectives in this paper, one of which is rather specific: to explain, theoretically, the molecular-elastic mechanisms governing the $L_\alpha \rightarrow H_{II}$ transition. The other, more general objective is to present the theoretical model used to explain this transition and describe its potential applications to other phenomena associated with (elasticity-driven) lipid-protein interaction, e.g., the role of protein size and shape in determining protein aggregation in lipid bilayers or helix tilt with respect to the membrane normal. Some aspects of these phenomena, especially the lipid-mediated protein interaction in bilayers, are necessary ingredients in the description of the $L_\alpha \rightarrow H_{II}$ transition and will unfold naturally in the course of our analysis.

Considerable theoretical effort has been devoted to the study of nonspecific (i.e., elastic) lipid-protein coupling and lipid-mediated protein-protein interactions. The variety of approaches include statistical lattice theories (Sperotto, 1997), microscopic and phenomenological molecular models (Fattal and Ben-Shaul, 1993; Marcelja, 1976; Mouritsen and Bloom, 1984), molecular dynamics simulations (Chen et al., 1997), as well as continuum theories of long-range interactions between inclusions driven by membrane fluctuation (Goulian et al., 1993). Several other models are based on continuum elastic theories, treating the membrane as a layer of a smectic liquid crystal with boundary conditions dictated by the size and shape of the hydrophobic inclusions (Helfrich and Jakobsson, 1990; Huang, 1986; Nielsen et al., 1998). Variational minimization of the elastic free energy functional, subject to these boundary conditions, then yields the optimal profile of the membrane interface and the magnitude of the interaction energy. Several continuum elastic models emphasize the role of the bending and stretching characteristics of the membrane, especially the spontaneous curvature of the constituent lipid monolayers (Dan et al., 1993, 1994; Aranda-Espinoza et al., 1996). One important prediction of these theories, with important implications for the lateral organization of proteins in the membrane, is that under certain conditions the interaction potential between inclusions may exhibit one or more minima at finite separations between the inclusions. The optimal distance depends on the spontaneous curvature of the lipid monolayer and the hydrophobic mismatch. A related interesting conclusion is that the incorporation of a "nonmatching" inclusion into a lipid bilayer can actually relieve some of the elastic frustration energy associated with its formation from two monolayers of nonzero spontaneous curvature. This is the case, for instance, when a short inclusion is incorporated into a bilayer made of two monolayers of positive spontaneous curvature (Aranda-Espinoza et al., 1996).

Most of the theories mentioned above are based on the assumption of strong hydrophobic coupling between the protein and the membrane lipids. That is, the lipid chains surrounding the protein are assumed to adjust their length to bridge the hydrophobic mismatch and hence prevent the exposure of hydrophobic segments to water. Of course, this assumption sets an upper limit on the (normal) thickness of

the hydrophobic inclusion, namely, twice the length of a fully extended lipid chain.

Like previous theories of lipid-protein interaction, the theory presented in the next section is based on the assumption of strong hydrophobic coupling. Similarly, we treat the protein as a rigid hydrophobic inclusion that imposes stretching or compression boundary conditions on the neighboring lipid chains, as dictated by the requirement for hydrophobic matching. However, our model differs from earlier theories in two important respects. First, it employs a *molecular-level* free energy expression to describe the variations in lipid packing around and between inclusions. More explicitly, the local free energy per lipid molecule is expressed as a sum of three terms, accounting for the repulsive interaction between the polar headgroups, the hydrocarbon-water surface energy, and the lipid chain length. For the first two terms we use a familiar simple model of these "opposing forces" (Israelachvili, 1992; May and Ben-Shaul, 1995). The chain stretching/compression term is based on treating the hydrophobic tail as a short Gaussian chain. Our simple three-term model, can be cast in the form of a continuum elastic free energy. Familiar elastic constants such as the bending rigidity and spontaneous curvature can then be expressed in terms of the molecular interaction parameters.

The second difference between our model and previous ones is concerned with the calculation of the elastic deformation free energy associated with the presence of membrane proteins. As usual, we write the system free energy as an integral over local contributions and determine the equilibrium state by variational minimization of the free energy functional, subject to the boundary conditions imposed by the size, shape, and lateral distribution of the inclusions. However, unlike in previous models, where the free energy integral is minimized with respect to one variable, the membrane shape profile, our model involves two structural elastic degrees of freedom: the local *chain length* and *chain tilt*. The inclusion of the tilt degree of freedom in the free energy functional is not a merely technical elaboration of existing models; it arises naturally from the need to account for nonlamellar lipid morphologies, as well as to describe the membrane response to hydrophobic inclusions with skewed boundaries.

In the following section we introduce our molecular model, relate its parameters to the elastic layer properties, explain the evaluation of the inclusion-induced elastic membrane energy, and establish the $L_\alpha - H_{II}$ phase coexistence conditions. The Results and Discussion present numerical results for the interaction of inclusions in planar membranes, the formation of an inclusion free H_{II} phase, and the inclusion-induced $L_\alpha \rightarrow H_{II}$ transition.

THEORY

Consider a symmetrical, single-component lipid bilayer of (unperturbed) hydrophobic thickness $2b_0$ and embedded proteins or peptides of thickness $2d_P$. We shall treat the proteins as rigid hydrophobic inclusions, symmetrical with respect to reflection through the bilayer midplane and cylindrically symmetrical with respect to rotation around their long axis. More specifically, in addition to simple cylindrical inclusions, we shall also consider the vase-like and barrel-like inclusions depicted in Fig. 2.

The elastic deformation free energy of the lipid bilayer and related properties, such as the interfacial profile of the membrane, depend on the geometrical characteristics of the inclusions as well as their lateral distribution in the membrane plane. As in other models of lipid-protein interaction, we shall adopt a mean-field approximation, whereby the total perturbation free energy of the membrane is treated as a sum of single inclusion contributions (Dan et al., 1993, 1994; Aranda-Espinoza et al., 1996). More specifically, with each inclusion we associate a two-dimensional (Wigner-Seitz) cell and assume that the perturbation in lipid packing around the inclusion is radially symmetrical. The perturbation extends from r_A, the radius of the inclusion at the bilayer midplane, to a distance r_B, corresponding to the average "radius" of the cell. For convenience we may assume that the proteins form a 2D hexagonal lattice, as illustrated in Fig. 1, with $2r_B$ denoting the distance between nearest-neighbor inclusions. It should be noted that although hexagonal order is likely to appear in protein-rich membranes (small r_B), the mean-field and radial symmetry approximations improve as the density of inclusions decreases (large r_B).

Focusing on one cell of the lipid-protein membrane, we define a Cartesian coordinate system whose origin is located at the center of the cell, i.e., in the middle of the principal axis of the inclusion, with the z axis along the membrane normal and the x, y plane coinciding with the membrane midplane. Because the inclusions considered here are symmetrical with respect to reflection through the midplane, we may limit the discussion to one, say the "upper" ($z > 0$), lipid monolayer. As the perturbation free energy is radially symmetrical around the inclusion, we also introduce a cylindrical coordinate system, r, ψ, z with $r = (x^2 + y^2)^{1/2}$ and ψ denoting the azimuthal angle, i.e., $x = r \cos \psi$, $y = r \sin \psi$. We use this coordinate system to characterize the local perturbation of the lipid monolayer at a radial distance r from the center of the inclusion, as shown in Fig. 3. Two functions specify the perturbation: the (average) local chain
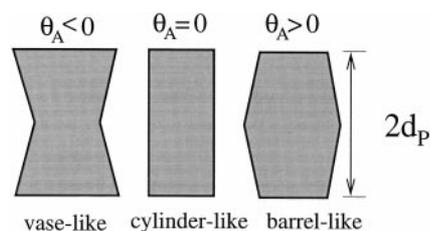
FIGURE 2 Cross sections, containing the principal axes, of vase-like, cylindrical, and barrel-like inclusions.
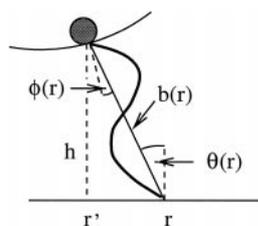
FIGURE 3 Local characteristics of a lipid molecule in a monolayer of a symmetrical bilayer. $b(r)$ is the average chain length, $\theta(r)$ is the tilt angle with respect to the bilayer midplane, and ϕ is the angle between the local chain director and the hydrocarbon-water interface.

length, $b(r)$, and the local tilt angle of the hydrophobic tails, $\theta(r)$. These functions, to be evaluated by functional minimization of the system's free energy, determine the local perturbation free energy and the hydrophobic thickness profile $h(r') = b(r) \cos \theta(r)$, where $r' = r - b(r) \sin \theta(r)$. Note that neither the effective lipid chain length nor the tilt angle is a static quantity for a bilayer in the liquid, disordered state. Rather, they result from an averaging over many different chain conformations. Note also that the effective lipid chain length, b, cannot exceed the maximal, all-*trans,* chain length b_{max}.

From the assumption of strong hydrophobic coupling discussed in the previous section, it follows that the lipid chains surrounding the inclusion must either stretch or compress, and if necessary tilt, to prevent the exposure of hydrophobic regions to water. In our model this implies the boundary conditions $b(r = r_{\mathrm{A}}) = d_{\mathrm{P}}/\cos \theta_{\mathrm{A}}$ and $\theta(r_{\mathrm{A}}) = \theta_{\mathrm{A}}$, with θ_{A} denoting the angle between the inclusion surface and the normal to the bilayer midplane.

The elastic deformation free energy of the membrane per inclusion (F) can be expressed as an integral over local contributions, $\Delta f(r) = f(r) - f_0$, where $f(r)$ is the free energy per molecule (whose tail end is) at r, and f_0 is the free energy per molecule in the inclusion-free membrane. Our molecular-level model of $f(r)$ takes into account all of the relevant lipid-lipid and lipid-solvent interactions. These interactions depend explicitly on the local chain length, $b(r)$, and tilt angle, $\theta(r)$. This will enable us to express ΔF as a functional of $b(r)$ and $\theta(r)$, as described next.

Molecular free energy

The average free energy per molecule in a self-assembled lipid bilayer, $f = F/N$, can be expressed as a sum of three terms: $f = f_{\mathrm{h}} + f_{\mathrm{i}} + f_{\mathrm{c}}$.

The first contribution is generally repulsive, resulting from electrostatic and/or steric interactions between the lipid polar heads. This term favors large areas per headgroup and will be modeled here by the familiar simple form $f_{\mathrm{h}} = B/a_{\mathrm{h}}$ (Israelachvili, 1992). In this expression a_{h} is the average area per headgroup, measured in the plane where, on average, headgroup repulsion is at maximum. The molecular constant B, which measures the strength of the repulsion, depends on the molecular characteristics of the

lipid headgroup, such as its size, shape, and charge. We shall use l_{h} to denote the distance between the plane of headgroup repulsion and the hydrocarbon-water interface where the area per molecule is a_{i}; in a planar membrane, $a_{\mathrm{h}} = a_{\mathrm{i}}$.

The second term in the molecular free energy, f_{i}, represents the surface energy associated with the hydrocarbon-water interface. The bilayer tends to minimize this unfavorable contribution by lowering the contact area between the hydrophobic core and the aqueous solvent, resulting in effective attraction between the lipid molecules. For this term we shall use another simple expression, $f_{\mathrm{i}} = \gamma a_{\mathrm{i}}$, where γ is the effective surface tension at the water-hydrocarbon interface (Tanford, 1980; Israelachvili, 1992), commonly estimated to be $\gamma = 0.12 k_{\mathrm{B}} T / \text{Å}^2$ at room temperature; T is the temperature and k_{B} is Boltzmann's constant.

The last contribution to the molecular free energy, f_{c}, accounts for the interaction between the lipid tails within the hydrophobic interior of the membrane. This term involves two contributions: 1) the cohesive (van der Waals) attraction between tail segments responsible for the membrane integrity and 2) the *repulsive* interaction between the lipid tails, reflecting the loss of conformational entropy associated with the tight packing (and hence stretching of the otherwise flexible) hydrocarbon chains. The cohesive bulk energy depends on the density of chain segments within the hydrophobic core. In the disordered fluid state of the membrane, this density is uniform and liquid-like throughout the core; hence the cohesive energy is constant and, for convenience, may be set equal to zero. The conformational free energy contribution to f_{c} plays an important role in determining amphiphile packing properties, membrane elasticity, and lipid-protein interaction characteristics (for a review see, e.g., Ben-Shaul, 1995). It may be noted, however, that in many standard treatments of amphiphile self-assembly, the conformational entropy contribution to f is neglected, resulting in the simple free energy expression $f = f_{\mathrm{i}} + f_{\mathrm{h}} = \gamma a_{\mathrm{i}} + B/a_{\mathrm{h}}$, also known as the "opposing forces" model (Israelachvili, 1992). The balance between the opposing forces (headgroup repulsion and interfacial attraction), supplemented by chain packing and translational entropy considerations, provides a simple and useful scheme for predicting the optimal aggregation geometry (e.g., planar bilayer versus cylindrical micelle) of a particular amphiphile. The additional repulsive interaction embodied in f_{c} plays a decisive role in our present molecular model, as outlined next.

The chain conformational energy has previously been determined using a statistical-thermodynamic mean-field theory of chain packing in various amphiphilic aggregates (Ben-Shaul, 1995). Here we opt for a much simpler scaling expression for f_{c}. Treating the hydrocarbon tails in the (orientationally ordered, melt-like environment of the hydrophobic core as a Gaussian chain, the conformational free energy scales with the effective chain length as $f_{\mathrm{c}} \approx b^2$ (deGennes, 1979; Gelbart and Ben-Shaul, 1987). We have previously shown that this scaling behavior, although

strictly appropriate only in the long chain limit, provides good agreement with membrane elastic properties calculated by the more elaborate molecular theory mentioned above, as well as with available experimental findings (May and Ben-Shaul, 1995). Adopting this scaling form for f_c, we arrive at the molecular free energy expression

$$f = \gamma a_i + \frac{B}{a_h} + \tau b^2 \qquad (1)$$

where τ measures the energetic cost associated with chain stretching.

In the planar bilayer geometry $a_i = a_h = a$ and $b = v/a$, where v is the volume of the hydrophobic tail. Let a_0 and $b_0 = v/a_0$ denote, respectively, the equilibrium values of the area per headgroup and chain length in the planar membrane. Using these quantities, it is convenient to define the reduced (dimensionless) constants

$$\bar{B} = Bb_0^2/(\gamma v^2), \quad \bar{\tau} = b_0^3\tau/(\gamma v), \quad \bar{l}_h = l_h/b_0 \qquad (2)$$

The equilibrium thickness of the protein-free planar monolayer, b_0, is determined by the minimum of f with respect to b. Equation 1 does not yield a general closed-form expression for b_0. Yet, a simple and useful relationship between $\bar{B}$ and $\bar{\tau}$, involving b_0, can be obtained by considering a small uniform stretching (or compression) deformation of the monolayer, whereby its thickness changes from b_0 to b. Expanding f around its minimum, $f_0 = f(b_0)$, in the planar configuration ($a_i = a_h = v/b$), we find that to first order in thickness variations,

$$\frac{b_0}{\gamma v}f = \frac{b_0}{\gamma v}f_0 + \frac{b - b_0}{b_0}(\bar{B} + 2\bar{\tau} - 1) \qquad (3)$$

with $(b_0/\gamma v)f_0 = 1 + \bar{B} + \bar{\tau}$. Clearly, the requirement for b_0 to be the equilibrium thickness is

$$\bar{\tau} = \frac{1 - \bar{B}}{2} \qquad (4)$$

which, upon substituting $\bar{B}$ and $\bar{\tau}$ as defined in Eq. 2, constitutes an equation for b_0. This equation implies that $0 \le \bar{B} \le 1$. In the limit $\bar{B} \to 1$, corresponding to $\bar{\tau} \to 0$, chain-chain repulsion is negligible compared to head-head repulsion, resulting in $b_0/v = 1/a_0 = (\gamma/B)^{1/2}$. In the opposite limit, $\bar{\tau} = \frac{1}{2}$, the equilibrium thickness is $b_0 = (\gamma v/2\tau)^{1/3}$.

Equation 1, considered so far only for a pure and planar lipid monolayer, is our basic expression for the local molecular free energy in both the L_α and H_{II} phases, with and without embedded inclusions. The presence of inclusions in these phases introduces local variations in the thickness and interfacial curvatures of their constituent monolayers, implying that b, a_i, and a_h are no longer constant. The extent of these variations, as well as the conditions favoring the $L_\alpha \to H_{II}$ transition, depends on the elastic response of the membrane to the presence of inclusions. The elastic properties of membranes are usually expressed and measured in

terms of elastic moduli defined via continuum theories. In the next section we establish the relationships between these phenomenological elastic constants and the molecular constants appearing in Eq. 1.

Elastic monolayer properties and molecular constants

The quantities B, τ, and l_h are not directly accessible by experiment. Rather, amphiphilic layers are generally characterized in terms of the equilibrium area per molecule, a_0, the spontaneous curvature, c_0, the bending rigidity, k, and the area compressibility modulus, λ, as defined by the familiar Helfrich elastic free energy (Helfrich, 1973). To leading order in the deviations from the equilibrium area, $a - a_0$, and cylindrical curvature, $c - c_0$, the elastic energy associated with such deformations is given by

$$\frac{f}{a_0} = \frac{f_0}{a_0} + \frac{1}{2}k(c - c_0)^2 + \frac{1}{2}\lambda\left(\frac{a}{a_0} - 1\right)^2$$
$$+ \chi(c - c_0)\left(\frac{a}{a_0} - 1\right) \qquad (5)$$

where $f_0 = f(a_0, c_0)$ is the free energy per molecule in the monolayer equilibrium configuration. Recall that, by symmetry, the spontaneous curvature of a symmetric *bilayer* is identically zero, and the elastic moduli, k, λ, and χ, are twice the monolayer values.

The areas, a, a_0, and curvatures, c, c_0, in Eq. 5 are measured with respect to an arbitrary ("dividing") surface within (or even outside) the monolayer, for example, the surface located at a distance δ from the hydrocarbon-water interface, as illustrated in Fig. 4. All of the constants in Eq. 5, (k, c_0, etc.) depend on the choice of this surface and hence on δ. Although sometimes implicitly, experimentally reported values of the elastic constants refer generally to one particular dividing surface, known as the *neutral surface*. By definition, area and curvature deformations measured with respect to the neutral surface are fully decoupled, i.e., Eq. 5 does not contain the cross term $(c - c_0)(a/a_0 - 1)$. In other words, the position of the neutral surface and, conse-
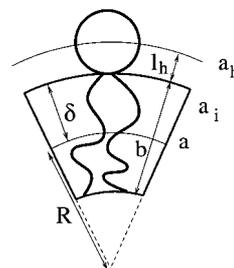
FIGURE 4   A segment of a cylindrically bent monolayer containing one molecule. The monolayer curvature $c = 1/R$ and area per molecule a are measured at an arbitrary surface, at distance δ from the hydrocarbon-water interface.

quently, the "decoupled" elastic constants are determined by the condition $\chi \equiv 0$.

Our goal now is to relate the molecular constants appearing in our molecular free energy expression, Eq. 1, with the elastic constants defined by Eq. 5. To this end a_h, a_i, and b of Eq. 1 should first be expressed in terms of the area and curvature of one particular surface. After Eq. 1 is expanded as a power series in these variables, the elastic constants can be evaluated by comparing the appropriate coefficients with those in Eq. 5. It must be noted, however, that unlike Eq. 5, the molecular expression in Eq. 1 is not restricted to small elastic deformations. In particular, we shall use Eq. 1 for both the planar bilayer (L_α) state where $c = 0$ and the inverse hexagonal (H_{II}) phase where the monolayer curvature is large and (by definition) negative: $c = c_H \approx -1/R$, where R is the radius of the water tubes (see Fig. 1). Clearly, the Helfrich expression, Eq. 5, is strictly valid either around the planar geometry (for $c_0 \approx 0$) or around the hexagonal state (when $c_0 \approx -1/R$), but not both. Nevertheless, as our goal here is just to provide an approximate correlation between the molecular and elastic constants, we shall assume (as is often done) that Eq. 5 applies to all relevant curvatures. Technically, this implies, for example, that $a_0 = v/b_0$ can be derived using $(\partial f/\partial a) = 0$ evaluated at $c = 0$ rather than at $c = c_0$. Similarly, in this approximation, $kc_0 = -(\partial(f/a_0)/\partial c)_{a_0, c=0}$ and $ka_0 = (\partial^2 f/\partial c^2)_{a_0, c=0}$.

Simple geometry relates a_h and a_i to the area per molecule at the neutral surface, a:

$$a_i = a(1 + \delta c), \quad a_h = a(1 + (\delta + l_h)c) \tag{6}$$

where, again, c is the curvature at the neutral surface. Moreover, b, the chain length in the bent monolayer, is simply related to the chain length v/a in the planar configuration, namely,

$$b = (v/a)\left[1 + c\left(\frac{(v/a)}{2} - \delta\right) + \frac{c^2}{2}\left((v/a)^2 - 3(v/a)\delta + 2\delta^2\right)\right] \tag{7}$$

In deriving this relationship we have assumed that the chain volume v does not change in the course of bending and have ignored terms of order higher than c^2.

Following the procedure outlined above, we obtain a number of useful relationships. The equation governing the equilibrium area per molecule, $a_0 = v/b_0$, is found to be $\bar{\tau} = (1 - \bar{B})/2$, as in Eq. 4. For the area compressibility modulus we get

$$\lambda = \gamma(3 - \bar{B}) \tag{8}$$

From the condition $\chi = 0$ we find the position of the neutral surface,

$$\delta = b_0 \frac{\frac{3}{2}(1 - \bar{B}) - \bar{B}\bar{l}_h}{3 - \bar{B}} \tag{9}$$

Using this result in the expressions derived for k and c_0, we obtain their forms in the neutral surface:

$$k = \frac{\bar{B}b_0^2\gamma[2(6 - 5\bar{B})\bar{l}_h^2 + (1 - \bar{B})(5 + 14\bar{l}_h)]}{2(3 - \bar{B})} \tag{10}$$

$$c_0 = \frac{(3 - \bar{B})(\bar{B}(1 + 2\bar{l}_h) - 1)}{\bar{B}b_0[2(6 - 5\bar{B})\bar{l}_h^2 + (1 - \bar{B})(5 + 14\bar{l}_h)]}$$

Although somewhat cumbersome, these results are useful for deriving numerical estimates for $\bar{B}$ and $\bar{\tau}$, using experimentally determined elastic constants (see the Results). Qualitatively, we expect that when interlipid repulsion is dominated by headgroup interactions (i.e., $\bar{B} \to 1$), the neutral surface will be located between the hydrocarbon-water interface and the headgroup surface; i.e., $\delta < 0$. Similarly, $\delta > 0$ is expected when chain-chain interactions dominate the repulsion. Indeed, as $\bar{B}$ and/or $\bar{l}_h$ decreases, a cross-over from negative to positive δ occurs at $\bar{B}(1 + 2\bar{l}_h/3) = 1$. The spontaneous curvature behaves similarly but changes sign at a somewhat different point, $\bar{B}(1 + 2\bar{l}_h) = 1$. (The sign changes of δ and c_0 need not be simultaneous.)

Area and (mean) curvature variations are not the only "normal modes" of membrane elasticity. For instance, in the discussion above we have totally ignored the Gaussian curvature associated with saddle-splay deformations (Helfrich, 1973), because they are irrelevant for the present analysis. On the other hand, changes in the chain tilt angle, θ (see Fig. 3), play a major role in our model, through the last term in Eq. 1. On average, in an unperturbed lipid monolayer, the equilibrium value of this angle is $\theta_0 = 0$. In the phenomenological theory of membrane elasticity, tilt deformations can be accounted for by adding, on the right-hand side of Eq. 5, a term of the form (Hamm and Kozlov, 1998)

$$\frac{f^{\text{tilt}}}{a_0} = \frac{\kappa}{2}\theta^2 \tag{11}$$

where κ denotes the *tilt modulus*. Again, using our molecular free energy expression, Eq. 1, and Eqs. 2 and 4, we find

$$\kappa = 2\tau b_0^2 = \frac{\gamma v}{b_0}(1 - \bar{B}) \tag{12}$$

Thus the tilt modulus is determined exclusively by the resistance, τ, of the alkyl chains to changes in their length. Indeed, changing θ at constant $a = a_0$ is entirely equivalent to chain stretching.

Inclusion-induced membrane deformation energies

Using the molecular free energy, Eq. 1, we now turn to the calculation of the elastic deformation energy associated with the incorporation of inclusions into a lipid membrane. Recall our assumption that the lipid perturbation zone prescribed by a cylindrically symmetrical inclusion is circular,

extending from r_A to r_B; r_A denotes the radius of the inclusion at the bilayer midplane and $2r_B$ the average distance between inclusions. Later on, when discussing the peptide-containing H_{II} phase, we shall need to consider lipid perturbation profiles corresponding to "*one-dimensional*" inclusions, i.e., inclusions whose surface appears to the boundary lipids as an infinite, membrane-spanning wall (either parallel or slanted with respect to the membrane normal). These *1D systems* can be treated as special cases of the corresponding cylindrically symmetrical *2D inclusions,* in the limit $r_B - r_A \ll r_A$. Let us first discuss the 2D systems, i.e., cylindrical inclusions in planar bilayers.

The elastic perturbation free energy of the bilayer, per inclusion, is given by

$$F_{el}^{B} = 2 \int \Delta f(r, \psi) dn \qquad (13)$$

$$= \frac{4\pi}{v} \int_{r_A}^{r_B} \Delta f(r) g_V(r) r \, dr = 4\pi\gamma \int_{r_A}^{r_B} \bar{f} r \, dr$$

where $\Delta f = f - f_0$ is the local perturbation free energy, per molecule, relative to the equilibrium state in the peptide-free planar monolayer, i.e., $f_0/\gamma a_0 = 1 + \bar{B} + \bar{\tau}$ see (Eq. 3). The integration in the first equality extends over all of the lipid molecules belonging to one of the two monolayers (hence the factor of 2) within the "unit cell" corresponding to one inclusion. Specifically, $dn = dV/v$ denotes the number of lipid molecules whose chain ends are located within the area element, $r \, dr \, d\psi$, centered around point r, ψ of the bilayer midplane. We use dV to denote the (3D) volume occupied by these dn chains within the hydrophobic core and express it in the form $dV = g_V(r) \, r \, dr \, d\psi$, where $g_V(r)$ can be interpreted as the radial distribution function of chain ends in the bilayer midplane. Because of the cylindrical symmetry of the inclusion, g_V is independent of the azimuthal angle ψ, explaining the passage to the second equality. Note, however, that r and ψ specify only the position of the chain ends, whereas dV and hence $g_V(r)$ depend also on the length $b(r)$ and tilt angle $\theta(r)$ of these chains (Fig. 3). These as yet unknown functions dictate the shape of the monolayer interfacial profile. The dimensionless function $\bar{f}(r)$, defined by the last equality in Eq. 13, can be interpreted as a local deformation energy of the monolayer per unit (midplane-projected) area. Finally, the total number of lipid molecules, per inclusion, is

$$n^B = \frac{4\pi}{v} \int_{r_A}^{r_B} g_V(r) r \, dr \qquad (14)$$

In addition to the volume differential $dV(r; b, \theta)$ defined above, we define $dA(r; b, \theta)$ as the differential area in the hydrocarbon-water interface, corresponding to the area element $r \, dr \, d\psi$ of the bilayer midplane. With these definitions the local molecular areas at the hydrocarbon-water interface $a_i(r) = a_i(r; b, \theta)$ and the headgroup surface

$a_h(r) = a_h(r; b, \theta)$ can be expressed in the form $a_i(r) = v \, dA(r, b, \theta)/dV(r, b, \theta)$ and $a_h(r) = v \, dA(r, b + l_h, \theta)/dV(r, b, \theta)$. In writing these expressions, we have used the assumption that the uniform (liquid-like) chain segment density within the lipid regions of the hydrophobic core is not affected by the presence of inclusions; this implies the equalities $a_i = dA_i/dn = v \, dA_i/dV$ and $a_h = dA_h/dn = v \, dA_h/dV$.

In analogy to $g_V(r; b, \theta)$ defined above, we define a "radial surface function," $g_A(r; b, \theta)$ through $dA(r; b, \theta) = g_A(r; b, \theta) r \, dr \, d\psi$. Explicit expressions for $g_V(r; b, \theta)$ and $g_A(r; b, \theta)$ are derived in Appendix A (see Eq. 28).

We turn now to the "1D inclusion model." To realize its structure, consider a lipid bilayer containing a periodic array of infinite hydrophobic walls, aligned parallel to the membrane y axis. The width of each wall, at the bilayer midplane, is $2x_A$, and the distance between walls is $2x_B$; their height along the membrane normal direction (z) is d_P. We shall keep using the terms "vase-like," "cylinder-like," and "barrel-like" inclusions to describe 1D inclusions whose cross sections appear (in the x, z plane) as in Fig. 2. Choosing a Cartesian coordinate system originating at (some point on) the center line of one inclusion, x_A marks the inclusion boundary and x_B half the distance to the next wall. A membrane region of size $2L \times x_B$ will be defined as a "unit cell" of the 1D model; L denotes the length of a wall segment along the y axis. One possible application of the 1D model involves the calculation of the lipid-mediated interaction between a pair of nearby large inclusions, corresponding to $r_B - r_A \ll r_A$ in the 2D model. In this limit the radial symmetry assumption of the 2D model is no longer valid, whereas the 1D picture is most appropriate. However, our main use of the 1D model concerns the calculation of the elastic free energy of the peptide-rich H_{II} phase. This application requires a slight but straightforward modification of the definition of the unit cell, as described in the next section.

The elastic deformation free energy of the lipid bilayer, per unit cell (or "per inclusion") in the 1D model is

$$F_{el}^{1D} = 4 \int \Delta f(x) dn = \frac{4L}{v} \int_{x_A}^{x_B} \Delta f(x) g_V(x) dx = 4\gamma L \int_{x_A}^{x_B} \bar{f}(x) dx \qquad (15)$$

with the dn integration involving all of the lipids in one-quarter of the unit cell, i.e., in a monolayer of area $L \times (x_B - x_A)$. The number of lipids in the unit cell is

$$n^{1D} = 4 \frac{L}{v} \int_{x_A}^{x_B} g_V(x) dx \qquad (16)$$

The functions $g_V(x)$ and $\bar{f}(x)$ are the 1D analogs of the corresponding quantities in Eq. 13. Similarly, the local interfacial areas $a_i(x)$, $a_h(x)$ are defined in analogy to $a_i(r)$, $a_h(r)$, with $dV = L \, dx \, g_V(x)$ and $dA = L \, dx \, g_A(x)$. Explicit expressions for $g_V(x)$ and $g_A(x)$ are obtained from $g_V(r)$ and

$g_A(r)$ (Appendix A) upon taking the limit $x = r \rightarrow \infty$, and noting that $\theta = \theta(x)$, $b = b(x)$. (This follows from the fact that as $r_A \rightarrow \infty$, all of the lipids within the perturbation region, $r_A \leq r \leq r_B$, interact with an essentially straight inclusion wall.)

Another useful characteristic of the perturbed lipid layer is the angle, ϕ, between the local chain director (average end-to-end vector) and the local normal to the monolayer interface (see Fig. 3). In terms of b and θ and their derivatives (primed), this angle is given by

$$\phi = \theta - \arctan\left(\frac{b' \cos \theta - b\theta' \sin \theta}{1 - b' \sin \theta - b\theta' \cos \theta}\right) \quad (17)$$

In the special case where $\phi = 0$, the chains point normal to the hydrocarbon-water interface, and the two degrees of freedom, b and θ, are no longer independent of each other. From Eq. 17 we find for $\phi = 0$,

$$b' = \sin \theta \quad (18)$$

We are now ready to evaluate the elastic deformation free energy F_{el}^B (Eq. 13). Let $s(r) = b(r)/b_0 - 1$ and $\theta(r)$ denote, respectively, the local deviations in the lipid chain length and tilt angle, from their equilibrium values in the unperturbed monolayer. Assuming that the membrane deformations are small, we express the free energy density, $\bar{f}$, as a second-order power series in $s(r)$, $s'(r)$, $\theta(r)$, and $\theta'(r)$, obtaining

$$\bar{f} = b_3\theta + b_4\theta' + a_{11}s^2 + a_{13}s\theta + a_{14}s\theta' + a_{22}s'^2 + a_{23}s'\theta$$
$$+ a_{33}\theta^2 + a_{34}\theta\theta' + a_{44}\theta'^2 \quad (19)$$

where $b_4 = b_0(\bar{B}(1 + 2\bar{l}_h) - 1)/2$, $b_3 = b_4/r$, $a_{11} = (3 - \bar{B})/2$, $a_{14} = b_0(\bar{B}(1 + 2\bar{l}_h) - \bar{\tau})$, $a_{13} = a_{14}/r$, $a_{22} = b_0^2(1 - \bar{B})/2$, $a_{23} = b_0(\bar{B} - 1)$, $a_{33} = (1 - \bar{B})/2 + \bar{B}b_0^2(1 + 2\bar{l}_h)^2/(4r^2)$, $a_{34} = b_0^2(1 + 2\bar{B}\bar{l}_h^2)/(2r)$, and $a_{44} = \bar{B}b_0^2(1 + 2\bar{l}_h)^2/4$.

The Euler-Lagrange equations corresponding to the minimization of $\int \bar{f}r \, dr$ are given by

$$s'' = \frac{(a_{14} - a_{23})(\theta + r\theta')}{2a_{22}r} + \frac{a_{11}}{a_{22}}s - \frac{s'}{r}$$

$$\theta'' = \frac{a_{23} - a_{14}}{2a_{44}}s' + \frac{a_{33}}{a_{44}}\theta - \frac{\theta'}{r}$$

Substituting the explicit expressions above for the various expansion coefficients and using Eq. 4 for $\bar{\tau}$, we find

$$s'' = \frac{\bar{B} - 3}{b_0^2(\bar{B} - 1)}s - \frac{1}{r}s' + \frac{1 + \bar{B}(1 + 4\bar{l}_h)}{2b_0(1 - \bar{B})}\left(\frac{\theta}{r} + \theta'\right) \quad (20)$$

$$\theta'' = -\frac{1 + \bar{B}(1 + 4\bar{l}_h)}{b_0\bar{B}(1 + 2\bar{l}_h)^2}s' + \left[\frac{1}{r^2} + 2\frac{1 - \bar{B}}{b_0^2\bar{B}(1 + 2\bar{l}_h)^2}\right]\theta - \frac{\theta'}{r}$$

By solving Eq. 20 numerically, subject to the appropriate boundary conditions, we can determine the stationary solutions for the interfacial profile of the perturbed monolayer,

the tilt angle profile, and, using $\bar{f}(r; b(r), \theta(r))$ in Eq. 13, the membrane deformation free energy. The boundary conditions reflect the shape of the inclusion envelope as well as the symmetry of the system in question. In detail, the boundary conditions at the inclusion surface are $\theta(r_A) = \theta_A$ and $s(r_A) = s_A$. The first boundary condition dictates the tilt angle of the lipids touching the inclusions. The second ensures perfect hydrophobic matching between the boundary lipids and the inclusion. The boundary conditions for a bilayer membrane at r_B are dictated by symmetry, $s'(r_B) = 0$ and $\theta(r_B) = 0$. Replacing r_A, r_B with x_A, x_B, we obtain the boundary conditions for 1D inclusions embedded in planar lipid bilayers.

Recall that the peptide-induced $L_\alpha \rightarrow H_{II}$ transition results in a peptide-rich hexagonal phase (Killian et al., 1996; Morein et al., 1997; Killian, 1992). The most likely arrangement of the peptides in this phase is as shown in Fig. 1, with the densely packed peptides forming a hydrophobic strip bridging adjacent water tubes. To a good approximation, these strips can be treated as one-peptide-wide 1D walls, as shown in Fig. 5 (*left*). The figure on the right shows (one-half of) the "unit cell" corresponding to this structure. Along the x axis the lipid (chain end) positions vary between x_A and $x_B = \lambda/2\sqrt{3}$, where λ denotes the lattice constant of the H_{II} phase (see Fig. 5, *right*). The special but important case of a peptide-free H_{II} phase simply corresponds to $x_A = 0$.

The boundary conditions on lipid packing in this 1D model of the H_{II} phase are as follows. At x_A, in the peptide-rich system, we have the usual chain length and tilt angle matching conditions: $s(x_A) = s_A$ and $\theta(x_A) = \theta_A$. In the pure H_{II} phase the boundary conditions at x_A are dictated by symmetry, i.e., $s'(x_A) = 0$ and $\theta(x_A) = 0$. At x_B the boundary conditions are the same for both cases:

$$\phi(x_B) = 0 \quad \theta(x_B) = \pi/6 \quad (21)$$

where ϕ is the angle defined in Eq. 17. The boundary condition $\phi(x_B) = 0$ expresses the fact that the chains pointing toward "interstitial axes" within the hydrophobic region of the H_{II} phase must not be tilted, thus guaranteeing a smooth hydrocarbon-water surface. Using Eq. 18, the condition $\phi(x_B) = 0$ can be rewritten as $s'(x_B) = 1/2b_0$. The only difference between the unit cell defined here for the 1D model of the H_{II} phase and the 1D model defined earlier for the bilayer phase is in the boundary conditions at x_B (that is,
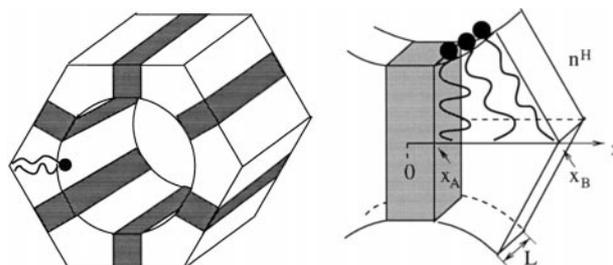
FIGURE 5   The 1D model of the inclusion-rich H_{II} phase.

$\theta(x_B) = \pi/6$ versus $\theta(x_B) = 0$ and $s'(x_B) = 1/2b_0$ versus $s'(x_B) = 0$).

The local perturbation free energy and the Euler-Lagrange equations for the 1D model are obtained from Eqs. 19 and 20, respectively, in the $r \rightarrow \infty$ limit. (Note that in this limit $b_3 = a_{13} = a_{34} = 0$.) Solving the Euler-Lagrange equations subject to the boundary conditions above, we obtain the lipid chain length and tilt angle profiles in the H_{II} phase. The elastic deformation free energy and the number of lipids per unit cell can then be evaluated from Eqs. 15 and 16, respectively.

Two "technical" comments: 1) To relate the number of lipids in a unit cell of length L with the number of lipids per inclusion, n^H, we set $L = 2x_A$ and determine x_A by the requirement that the cross-sectional areas of the inclusion in the 1D and 2D models are equal, i.e., $\pi r_A^2 = (2x_A)^2$, and hence $L = 2x_A = \sqrt{\pi} r_A$. 2) Fig. 5 illustrates the 1D-H_{II} model for simple straight-cylinder inclusions; the extension of the model to inclusions with nonvanishing tilt angle (e.g., barrel-like) is straightforward.

L_{α}-H_{II} phase coexistence

Let N^H and M^H denote, respectively, the number of lipids and inclusions in the inverse hexagonal phase; N^B, M^B denote the corresponding quantities in the bilayer phase. As argued in previous sections, the inclusions in the peptide-rich H_{II} phase are assumed to be aggregated along the hexagonal tubules, spanning the hydrophobic region between neighboring water tubes. Thus each tubule involves six densely packed one-dimensional inclusion arrays (Fig. 5). On the other hand, we shall assume that the peptides are randomly dispersed in the peptide-poor bilayer phase. These assumptions will later be corroborated by our numerical results.

The total free energy of a solution containing lamellar and hexagonal aggregates in equilibrium with each other is given by

$$\mathcal{F} = M^H F^H(n^H) + M^B F^B(n^B) \qquad (22)$$

where $n^B = N^B/M^B$ and F^B denotes the number of lipids and the free energy, per inclusion, in the bilayer, etc. (Treating the bilayer and hexagonal aggregates as macroscopic phases, we ignore their translational entropy.)

Minimization of $\mathcal{F}$ with respect to $N^B = N - N^H$ and $M^B = M - M^H$ yields the phase equilibrium conditions, i.e., equality of the peptide and lipid chemical potentials in the coexisting phases. These conditions lead to the usual "common tangent" equations,

$$F^H(n^H) - F^B(n^B = n^H(\partial F^H/\partial n^H) - n^B(\partial F^B/\partial n^B)$$

$$(\partial F^H/\partial n^H) = (\partial F^B/\partial n^B) \qquad (23)$$

Because the concentration of peptides in the bilayer phase is small, F^B should include a mixing entropy term, F_{mix}, in

addition to the elastic deformation energy,

$$F^B(n^B) = F_{el}^B(n^B) + F_{mix}^B(n^B) \qquad (24)$$

Assuming ideal mixing (Guggenheim, 1949), we can write $F_{mix}^B/k_BT = \ln \rho_M^B + n^B \ln \rho_N^B$, where ρ_M^B and ρ_N^B are, respectively, the area fractions of inclusions and lipids in the L_{α} phase. In terms of n^B, the mixing free energy (in units of k_BT) is given by

$$F_{mix}^B(n^B) = \ln \frac{1}{1 + \alpha n^B} + n^B \ln \frac{\alpha n^B}{1 + \alpha n^B} \qquad (25)$$

where $\alpha = a_N/(2a_M)$; a_N and a_M denote the cross-sectional areas of the lipid and peptide molecules, respectively. The factor of 2 in the expression for α arises because each inclusion contributes to two monolayers.

Following our assumption that the inclusions in the H_{II} phase are densely packed and fixed in their lattice positions, we set $F_{mix}^H = 0$ and hence $F^H (n^H) = F_{el}^H(n^H)$.

Numerical results for F^H and F^B and the corresponding solutions of the coexistence conditions (Eq. 23) will be reported in the next section. These calculations show that, in general, F^H exhibits a deep minimum at some given lipid-inclusion concentration ratio $n^H = \hat{n}^H$, where $F^H = \hat{F}^H = F_{el}^H (\hat{n}^F)$. Under these conditions Eq. 23 reduces to a single equation,

$$\hat{F}^H - F^B(n^B) = (\hat{n}^H - n^B)(\partial F^B/\partial n^B) \qquad (26)$$

which determines the equilibrium value of n^B. It turns out that, in general, $n^B \gg 1$, i.e., the inclusions are far from each other, implying that $F_{el}^B(n^B) \rightarrow \hat{F}^B = constant$, where $\hat{F}^B$ is the elastic free energy associated with an isolated inclusion. The coexistence equation (Eq. 26) is then given by

$$\hat{F}^H - \hat{F}^B = F_{mix}^B(n^B) + (\hat{n}^H - n^B)(\partial F_{mix}^B/\partial n^B) \qquad (27)$$

The physical meaning of this equation is simple: the loss in mixing entropy associated with the transfer of one inclusion from the dilute bilayer phase to the ordered H_{II} phase is balanced by the gain in elastic deformation energy (which is lower) in the ordered hexagonal phase. A particularly simple and familiar form of this equation is obtained in the limit $n^B \gg 1$, corresponding to a very low density of inclusions in the bilayer. Namely, $\hat{F}^H = \hat{F}^B + \ln(1/\alpha n^B)$, expressing the usual condition (equality of chemical potentials) for the equilibrium partitioning of solutes (here the inclusions) between a "solid" (here the H_{II}) and a dilute "liquid" (L_{α}) phase; $(1/\alpha n^B)$ is the concentration of inclusions in this phase.

RESULTS AND DISCUSSION

In this section we report numerical calculations for several model systems. After a short introduction explaining the choice of the molecular parameters and model systems considered, we present the results in two parts. The first part

describes our calculations for lipid-mediated interactions between inclusions in planar bilayers. The second part focuses on the peptide-mediated $L_\alpha \rightarrow H_{II}$ transition. We shall also discuss the $L_\alpha \rightarrow H_{II}$ transition in pure lipid systems.

Molecular and elastic constants

All of the calculations reported below are based on the molecular free energy expression (Eq. 1). The choice of the molecular constants appearing in this expression, B and τ, was guided by general experimental information concerning more familiar membrane characteristics, such as the monolayer bending rigidity, k, spontaneous curvature, c_0, and average membrane thickness, b_0. Structural information was used for choosing other relevant parameters such as v and l_h.

In all of our calculations we have used $v = 2 \times 459 \, \text{Å}^3$, corresponding to lipids with hydrophobic tails consisting of two saturated C-16 = —(CH$_2$)$_{15}$ —CH$_3$ chains. The tail volume is calculated using $v_{CH_2} = 27 \, \text{Å}^3$ for the effective volume of a CH$_2$ segment and $v_{CH_3} \approx 2v_{CH_2}$ (Tanford, 1980). For the distance of the headgroup repulsion surface from the hydrocarbon-water interface we have used $l_h = 1.74 \, \text{Å}$, and for the tail repulsion coefficient $\tau = 0.004 k_B T / \text{Å}^2$. The headgroup repulsion constant, B, will serve as a control parameter allowing variations in k, c_0, and b_0.

Using the above values of v, l_h, and τ, we show in Table 1 how the relevant elastic constants vary with B. We note that as B decreases, 1) the area per molecule, $a_0 = v/b_0$, decreases (weaker lipid-lipid repulsion), 2) the bending rigidity increases (because chain repulsion is stronger as a_0 decreases; recall $k \approx b_0^2$; Eq. 10), and 3) the spontaneous curvature becomes increasingly negative, i.e., the monolayer tends to bend more toward the water phase (because the torque associated with headgroup repulsion becomes less efficient in balancing the torque of chain repulsion). It should be noted that negative spontaneous curvature is not a sufficient condition for thermodynamic preference of the hexagonal over the bilayer phase (see below).

The explicit inclusion of the chain-tilt degree of freedom in our model enables us to study systems where lipid tilt is either inevitable or likely to occur. For example, the presence of bulky amino acid side chains around an α-helical backbone may result in a hydrophobic envelope different from a simple straight cylinder. The *barrel-like* and *vase-like* inclusions depicted in Fig. 2 represent two prototypes of such structures.

TABLE 1 Monolayer equilibrium chain length, b_0, bending rigidity, k, and spontaneous curvature, c_0, as a function of the headgroup interaction constant B, for $l_h = 1.74 \, \text{Å}$

$B/k_B T \text{Å}^2$	$b_0/\text{Å}$	$k/k_B T$	$c_0^{-1}/\text{Å}$
413	14.0	6.0	∞
350	14.8	7.4	-141
320	15.3	8.1	-97
285	15.9	9.1	-72
200	17.5	11.7	-41

In our model the shape of the inclusion enters only through the boundary conditions for the Euler-Lagrange equations (Eq. 20). Two boundary conditions specify, respectively, the tilt angle, θ_A, and chain length, b_A, at the surface of the inclusion. Barrel-like, cylinder-like, and vase-like inclusions correspond to positive, zero, and negative θ_A, respectively. The chain length boundary condition reads $b_A = d_P/\cos \theta_A$, where $2d_P$ is the hydrophobic thickness of the inclusion (Fig. 2). The *hydrophobic mismatch* is generally defined as the difference $2(d_P - b_0)$. As a reduced measure of the hydrophobic mismatch, we shall use the dimensionless quantity $\bar{s}_A = (d_P/b_0 - 1)$. For a straight-cylinder inclusion ($\theta_A = 0$), $\bar{s}_A > 0$ ("positive mismatch") implies chain stretching around the inclusion, and $\bar{s}_A < 0$ ("negative mismatch") imposes chain compression. More generally, the chain length deformation at the inclusion boundary, $s_A = b_A/b_0 - 1$, is related to the hydrophobic mismatch by

$$\bar{s}_A = (s_A + 1)\cos \theta_A - 1$$

Finally, in all examples we shall consider inclusions of radius $\bar{r}_A = 4 \, \text{Å}$, as measured at their thinnest region (e.g., the waist of the vase-like peptide). Thus the inclusion radius at the position of the bilayer midplane is given by $r_A = \bar{r}_A$ for $\theta_A \leq 0$ and $r_A = \bar{r}_A + b_A \sin \theta_A$ for $\theta_A > 0$.

Inclusions in bilayers

We begin with a simple example: a symmetrical planar bilayer, containing a small number of well-separated cylindrical inclusions. Under these conditions the membrane perturbation energy is a sum of single-inclusion contributions. As a typical case we show in Fig. 6 the lipid perturbation profile corresponding to a system characterized by $B = 413 k_B T \, \text{Å}^2$ (hence $c_0 = 0$), $\theta_A = 0$, $r_B = 30 \, \text{Å}$ ($r_B \gg r_A = 4 \, \text{Å}$ ensures that the inclusions are far from each other), and $\bar{s}_A = -0.2$, i.e., negative mismatch. We see that although the inclusion is a straight cylinder, the membrane perturbation involves not only a change in the lipid chain lengths, b, but also in the tilt angle, θ. The gradual variation
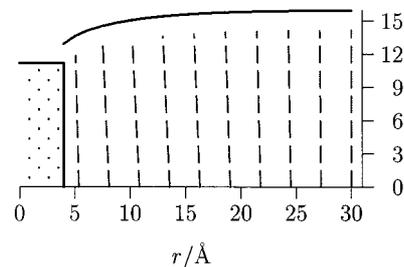
FIGURE 6 The monolayer perturbation profile resulting from the presence of an isolated cylindrical inclusion ($\theta_A = 0$, $r_B = 30 \, \text{Å}$). In this system $c_0 = 0$ ($B = 413 k_B T \, \text{Å}^2$), and the only cause for lipid perturbation is the (negative) hydrophobic mismatch, $\bar{s}_A = -0.2$. The solid line marks the hydrocarbon-water interface. The dashed lines drawn at several (arbitrary) positions represent the local chain director.

in θ alleviates the free energy penalty inflicted by the changes in lipid chain length. This coupling between the two lipid degrees of freedom allows for rapid relaxation of the perturbation profile. This prediction of the model agrees with previous, more detailed (yet much more difficult and limited) calculations, revealing that under similar mismatch conditions the range of perturbation around an isolated inclusion involves just a few lipid layers (Fattal and Ben-Shaul, 1993).

Effects of inclusion size and shape

The range and extent of chain length and tilt angle variations in Fig. 6 are quite moderate. Considerably more pronounced variations appear when the inclusions are not straight cylinders, when the hydrophobic mismatch is larger, and when the spontaneous monolayer curvature is nonzero. More interesting, however, are the perturbation free energies corresponding to all of these cases. Fig. 7 summarizes a series of calculations, showing the lipid-mediated interaction energies between several types of inclusions, embedded in two types of lipid bilayers. The figure shows how the elastic membrane energy per inclusion, F_{el}^B, varies with the 2D density of inclusions, as measured by the average half-distance between neighboring inclusions, r_B. The asymptotic ($r_B \rightarrow \infty$) values of F_{el}^B correspond to the perturbation free energies of isolated inclusions. The difference $F_{el}^B (r_B) - F_{el}^B(\infty)$ may be interpreted as the lipid-mediated interaction between inclusions.

In the left diagram of Fig. 7 we show the results for systems characterized by negative hydrophobic mismatch ($\bar{s}_A = -0.2$); the diagram on the right corresponds to positive mismatch ($\bar{s}_A = 0.2$). In each of the two diagrams we show free energy curves corresponding to the three prototypes (vase, cylinder, barrel) of inclusions ($\theta_A = -0.2$, 0, 0.2). Furthermore, because the membrane response to perturbations depends on its (monolayer) spontaneous curvature, the calculations were performed for two kinds of membranes. One corresponds to $c_0 = 0$ ($B = 413k_BT$ Å^2), and the other to $c_0 \approx -0.01$ Å^{-1}, ($B = 320k_BT$ Å^2) (see Table 1). In the latter case, the elastic free energy of the

inclusion-free bilayer is still lower than that of the inclusion-free inverse hexagonal phase, as shown below (see Fig. 9).

The most apparent qualitative conclusion from Fig. 7 is that the lipid-mediated interaction between inclusions depends strongly, both qualitatively and quantitatively, on their size and shape. Changing the monolayer spontaneous curvature from $c_0 = 0$ to $c_0 \approx -0.01$ Å^{-1} influences the magnitude of the elastic deformation energies, but not their qualitative behavior, as a function of r. (However, later on we will see that the value of c_0 plays a crucial role in determining whether the $L_\alpha \rightarrow H_{II}$ transition does or does not take place.)

For perfectly cylindrical inclusions the model predicts that the absolute minimum of F_{el}^B corresponds, always, to close contact between inclusions, i.e., $r_B = r_A$. Because the minimum is several k_BT's deep, it also predicts that these kinds of inclusions already tend to aggregate at room temperature. We note, however, that the free energy curves corresponding to cylindrical inclusions exhibit a barrier at some finite distance, $r_B > r_A$. Interestingly, any deviation from the straight-cylinder shape shifts the minimum in the interaction potential to $r_B > r_A$. Typically, long-range repulsions characterize the interaction between large vase-like inclusions and between small barrel-like inclusions. On the other hand, when the inclusions are small and vase-like or large and barrel-like, the minimum in F_{el}^B appears to be just a few Å away from r_A.

Tilt angle relaxation

One important respect distinguishing our model from previous models of lipid-protein interaction is the explicit inclusion of the tilt degree of freedom. That is, our free energy density, $\bar{f}$ (Eq. 19), is a function of two local variables: the chain length, b, and the tilt angle, θ, both allowing for membrane relaxation in response to the presence of a rigid inclusion. A direct test of the relative importance of chain tilt relaxation is provided by comparing the interaction free energy between inclusions with and without allowance for tilt relaxation. In the latter case a specific assump-

FIGURE 7 Membrane perturbation free energies, per inclusion (F_{el}^B), as a function of the half-distance between inclusions (r_B). The left and right diagrams are for inclusions corresponding to negative ($\bar{s}_A = -0.2$) and positive ($\bar{s}_A = 0.2$) hydrophobic mismatch, respectively. Curves a and d represent the results for cylinder-like inclusions ($\theta_A = 0$). b and e are for vase-like inclusions ($\theta_A = -0.2$). c and f are for barrel-like inclusions ($\theta_A = 0.2$). The solid curves correspond to $B = 413k_BT$ Å^2 ($c_0 = 0$), and dashed curves correspond to $B = 320k_BT$ Å^2 ($c_0 \approx -0.01$ Å^{-1}).
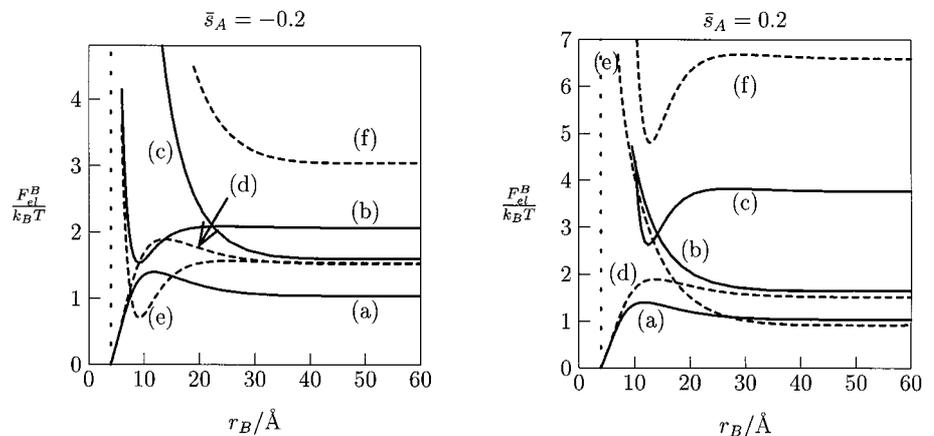
tion must be made concerning the functional dependence of θ on the distance between the interacting inclusions. The most natural choice is to assume that the local chain director is always perpendicular to the hydrocarbon-water surface; i.e., $\phi \equiv 0$ in Fig. 3, implying $\sin\theta = b'$ (see Eq. 18).

To simplify the analysis we shall compare the predictions of the 1D model, i.e., we consider the lipid-mediated interaction between two infinite and parallel inclusions, with $x_B - x_A$ denoting (half) the distance between them, at the bilayer midplane. Substituting $\theta \approx \sin\theta = b'$ in Eq. 19, the free energy density, $\bar{f}$, becomes a function of b and its derivatives:

$$\bar{f} = b_4 b_0 s'' + a_{11} s^2 + a_{14} b_0 s s'' + a_{44} b_0^2 s''^2,$$

with the coefficients as given after Eq. 19. Using this $\bar{f}$ in the variational minimization of the total deformation energy, F_{el}^{1D} in Eq. 15, we obtain the Euler-Lagrange equation $a_{11}s + b_0 a_{14} s'' + b_0^2 a_{44} s'''' = 0$. The relevant boundary conditions are $s(x_A) = s_A$, $s'(x_A) = \theta_A/b_0$, $s'(x_B) = 0$, and $s'''(x_B) = 0$.

As a special case demonstrating the role of the tilt angle, we have chosen a system with the following molecular characteristics: $B = 320k_BT\,\text{Å}^2$, $\bar{s}_A = -0.2$, and $\theta_A = -0.1$. The elastic deformation energies are shown in Fig. 8, where curves a and b refer to bilayers where tilt relaxation is allowed and arrested, respectively.

The difference between the two lipid-mediated interaction potentials is quite striking. First, as expected, the magnitude of the elastic deformation energy is significantly smaller when tilt relaxation is allowed to take place. Second, the shapes of the interaction potentials are qualitatively different. The oscillations characterizing the system where tilt relaxation is arrested are totally damped in the relaxed system. The origin of this difference lies partly in the shape of the inclusion. Without allowing for tilt relaxation, the lipid monolayers between the two vase-like inclusions must first bend toward the bilayer midplane, resulting in excessive compression of the already compressed lipid chains (because of the negative mismatch). For some systems, e.g., straight-cylinder inclusions, the effect of tilt relaxation may

be less pronounced. Clearly, however, the lipids' tilt degree of freedom plays an important role in determining the shape and magnitude of the elastic interaction between bilayer inclusions.

The $L_\alpha \rightarrow H_{II}$ transition

The most stable aggregation geometry of a given lipid in aqueous solution is dictated by an interplay between molecular force constants; in our model these are B, τ, and γ. In the phenomenological elastic theory of lipid layers, the relevant parameters are the elastic constants, such as k and λ, and the (monolayer) spontaneous curvature, c_0. For example, when $c_0 \approx 0$, the planar bilayer is the predominant phase because it involves the least (monolayer) frustration energy. On the other hand, when the lipid monolayer tends to curve "negatively," i.e., toward the water phase, the inverse hexagonal phase may be the predominant one (Seddon, 1990). By varying the external conditions (e.g., temperature, ionic strength), phase transitions can be induced between the bilayer and hexagonal phases, quite often through cubic mesophases that we shall not discuss here. Adding foreign molecules to the lipid matrix changes its elastic properties, resulting in changes in the phase transition characteristics. Hydrophobic peptides constitute a special, but important, class of foreign inclusions. In this section we will focus on the peptide-mediated $L_\alpha \rightarrow H_{II}$ transition in lipid systems, which, in the absence of peptides, form stable bilayers. Thus we shall first consider the "reference" peptide-free system.

Pure-lipid systems

The H_{II} phase is often depicted as an aggregate of cylindrically bent monolayers, with the lipid headgroups facing the hexagonally arranged water tubes. However, this picture is approximate because the hexagonal symmetry of the H_{II} phase "frustrates" the cylindrical symmetry of the lipid tails surrounding the water tubes. That is, whereas the lipid chains bridging between neighboring water tubes are somewhat compressed, those lipid tails that point toward the triangular regions of the hydrophobic core are necessarily stretched out. This nonuniform distribution of lipid chain lengths around the monolayer circumference is the origin of the elastic "frustration energy" in inverted lipid phases (Seddon, 1990). We shall see later that partial hexagonal faceting of the lipid-water interface can greatly relieve this unfavorable energy.

Ignoring for a moment the frustration energy, the propensity of lipids in water to self-assemble into the hexagonal rather than the bilayer phase may be assessed by comparing the elastic energies of the monolayers constituting these structures. Assuming that the area per molecule is the same in both phases, i.e., $a = a_0$, the two structures differ only in their curvature elastic energy, $f \propto (c - c_0)^2$ (see Eq. 5). In the bilayer $c = 0$, whereas in the hexagonal phase $c = c_H <$
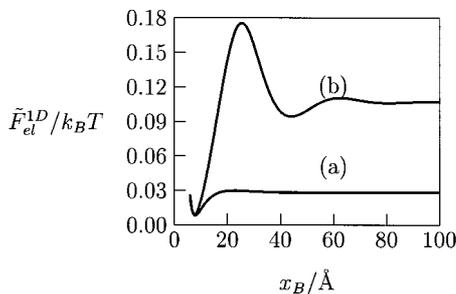
FIGURE 8 The lipid-mediated interaction between two infinite and parallel inclusions in a bilayer, with (a) and without ($\phi = 0$) (b) allowance for tilt relaxation. The calculations correspond to a system with $B = 320k_BT$ Å^2, $\bar{s}_A = -0.2$, $x_A = 4$ Å, and $\theta_A = -0.1$. ($\tilde{F}_{el}^{1D} = F_{el}^{1D}/2L$ is the elastic energy corresponding to one-half of a unit cell of length $L = 1$ Å.)

0, where typically $c_H \approx -1/30$ Å. Thus, for the hexagonal phase to be preferred over the bilayer, it is necessary that $(c_H - c_0)^2 < c_0^2$. This, in turn, implies that c_0 must be negative and that $|c_0| > |c_H|/2$; in other words, the monolayer spontaneous curvature should be "closer" to c_H than to $c_B = 0$. For typical H_{II} lipid phases this means $|c_0| > 1/60$ Å. If the above considerations were exact, then, based on the data in Table 1, we could conclude that once the headgroup force constant, B, falls below $\sim 250/k_B T$ Å^2, the C-16 lipid system will prefer the hexagonal over the bilayer phase. Detailed calculations of the elastic free energies in these phases are shown in Fig. 9, revealing that the critical value of B is $\sim 285/k_B T$ Å^2. Thus the H_{II} phase becomes dominant at values of c_0 that are less negative than those implied by simple curvature considerations.

The quantity shown in Fig. 9 is the elastic free energy difference, *per lipid molecule,* between the (pure-lipid) H_{II} and L_α phases,

$$\Delta \hat{f}_{el}^{B \to H} = F_{el}^H / n^H - f_{el}^B$$

The first term on the right-hand side of this equation, i.e., the average elastic energy per lipid in the H_{II} phase, depends on the hexagonal lattice parameter x_B (see Fig. 5). It should be noted that because the lipid tail length cannot exceed the length of the fully extended chain, a substantial increase in x_B implies a substantial faceting of the hexagonal water tubes, as shown in Fig. 10. Thus as x_B increases, an increasing fraction of the lipids in the hexagonal phase are actually packed in a bilayer-like environment, explaining why $\Delta \hat{f}_{el}^{B \to H} \to 0$ as $1/x_B \to 0$ (Fig. 9).

Regarding $1/x_B$ as the "order parameter" of the $L_\alpha \to H_{II}$ transition, one may interpret our model as predicting a *first*-order transition. (This behavior can be correlated with the fact that the monolayer-mediated "interaction potential" between the two hexagonal corners is that of a strongly damped oscillation.) It should be noted, however, that in practice, the transition may involve intermediate structures (Siegel and Epand, 1997) and thus different order parameters.

A typical faceting pattern of the lipid monolayer in the H_{II} phase is portrayed in Fig. 10. This particular pattern was calculated for a system with a strong preference for the hexagonal structure, as indicated by the small value of the
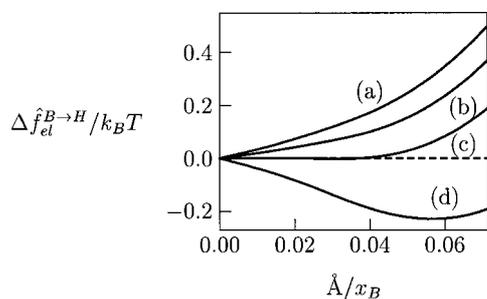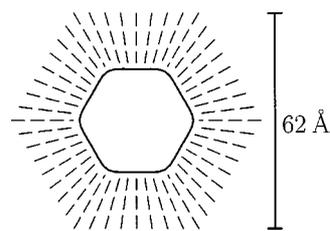
FIGURE 10   Two-dimensional projection of one "cylindrical" unit (water tube surrounded by lipid monolayer) of the H_{II} phase. The pattern shown was calculated using $B = 200 k_B T$ Å^2 and corresponds to the equilibrium value of the hexagonal lattice parameter, $\lambda = 62$ Å ($x_B = 18$ Å). The solid line marks the surface of headgroup interaction, and the dashed lines drawn at several (arbitrary) positions represent the local chain director.

headgroup repulsion constant, $B = 200 k_B T$ Å^2. The equilibrium value of the lattice parameter is $\lambda = 2\sqrt{3}x_B = 62$ Å, ($x_B = 18$ Å). Qualitatively, the origin of monolayer faceting or, more generally, the noncircular profile of the monolayer interface, is not difficult to explain. On the one hand, the monolayer tends to bend (negatively and uniformly) so as to minimize $|c_H - c_0|$ and hence the curvature elastic energy. This, in principle, can be achieved without chain tilting (i.e., $\phi = 0$), but at the cost of extensive chain stretching ("frustration") toward the hexagonal interstices. Because chain stretching is highly unfavorable, the monolayer attempts to achieve $b = b_0$ for as many chains as possible, including those that stretch toward the hexagonal interstices. This can only be achieved by extensive faceting and concomitant chain tilting ($\phi \neq 0$), resulting in hexagonally shaped water regions, as in Fig. 10 (Seddon, 1990). Based on these considerations, we expect that the extent of faceting will decrease as $\bar{B}$ increases relative to $\bar{\tau}$. It should be mentioned that another theoretical model has recently been proposed for the H_{II} phase, taking into account only the tilt degree of freedom (Hamm and Kozlov, 1998).

Experimental support for the above conclusions is provided by recent x-ray-based reconstitution studies of the H_{II} phase (Turner and Gruner, 1992). These experiments, pertaining to the H_{II} phase of dioleoylphosphatidylethanolamine (for $\lambda > 75$ Å), reveal a significant deviation of the monolayer profile from the circular symmetry.

The inclusion-induced $L_\alpha \to H_{II}$ transition

In this section we consider lipid systems which, in the absence of inclusions, form stable bilayers, but upon the addition of inclusions prefer the formation of an H_{II} phase. More specifically, we shall consider lipids whose spontaneous curvature is negative, yet not negative enough to stabilize an inclusion-free H_{II} phase. Thus the calculations reported below are for $B > 320 k_B T$ Å^2, implying $|c_0| < (1/100)$ Å^{-1}. We shall consider several inclusion shapes, all corresponding to negative hydrophobic mismatch, as our calculations show that long inclusions do not induce the $L_\alpha \to H_{II}$ transition.

FIGURE 9   The elastic free energy per molecule in the H_{II} phase, relative to the bilayer state. Curves *a–d* correspond to $B = 413, 350, 285$ and $200 k_B T$ Å^2, respectively.

In Fig. 7 we see that, in some cases, the lipid-mediated interaction between inclusions exhibits a distinct minimum at a certain, typically very small, inter-inclusion separation; e.g., for perfectly cylindrical inclusions a pronounced minimum appears at close contact. In these systems lateral phase separation is expected to take place once the 2D concentration of inclusions exceeds a certain (temperature-dependent) threshold value. This in-plane transition will be preempted by the $L_\alpha \rightarrow H_{II}$ or any other phase transition involving a lower threshold concentration. In the following analysis we shall assume that this is indeed the case with respect to the $L_\alpha \rightarrow H_{II}$ transition, or, in other words, we shall disregard the possibility that a 2D transition will compete with the lamellar-hexagonal transition. There is another reason for not considering here the 2D transition that is related to our model for calculating F_{el}^B. In these calculations we have assumed that every inclusion interacts with a radially symmetric distribution of its neighbors. Furthermore, a continuum theory was used to represent the free energy density ($\bar{f}$). Both the radial symmetry assumption and the continuum theory are valid at low peptide concentrations, i.e., at relatively large separations between inclusions. In Fig. 7 we see that the minima in F_{el}^B generally appear at very short distances ($2(r_B - r_A) \leq 20$ Å) corresponding to no more than about two lipid layers between inclusions. Because the applicability of our calculations in this range is questionable, we shall limit the use of F_{el}^B to those regions where the concentration of inclusions is small, say $n_B \geq 20$. It turns out that this is the relevant concentration regime for the $L_\alpha \rightarrow H_{II}$ transition. Experimentally, 2D protein aggregation within a planar bilayer is more abundant than the $L_\alpha \rightarrow H_{II}$ transition (Marsh, 1995; Ryba and Marsh, 1992). The fact that in some systems the transition to an inverted hexagonal phase preempts the 2D transition may partly be related to their inability to form extended 2D aggregates. Indeed, it has been suggested that in the systems studied by Killian et al. (1996), repulsive interactions between the interfacially anchored tryptophans prevent 2D peptide aggregation.

To find out whether the $L_\alpha \rightarrow H_{II}$ transition indeed takes place and, in case it does, to evaluate the lipid-inclusion concentration ratios in the two phases, one needs to solve the common tangent equations described in the Theory section.

In Fig. 11 we show, for two systems, F^H and F^B as functions of n, and the common tangent construction for determining the coexistence values of n_H and n_B (see Eq. 23). For both systems $B = 320k_B T$ Å^2, implying $c_0 \approx -1/100$ Å, (Table 1). Recall that for this value of c_0, the stable form of the inclusion-free system is the lipid bilayer. For both cases shown in Fig. 11, the hydrophobic mismatch is strongly negative: $\bar{s}_A = -0.35$ for the perfectly cylindrical inclusions ($\theta_A = 0$, *left diagram*) and $\bar{s}_A = -0.30$ for the slightly barrel-like inclusions ($\theta_A = 0.1$, *right diagram*). The free energy of the hexagonal phase was calculated using the 1D scheme, based on the structural model described in Fig. 5. We have used $x_A = (\sqrt{\pi}/2)r_A$, where $r_A = 4$ Å denotes the radius of the inclusion. In general, F^H and F^B can be expressed as functions of either the distance between inclusions (x_H or r_B) or the number of lipids per inclusion (n^H or n^B). Note, however, that the number of lipids per inclusion, e.g., n^H, depends not only on x_H, but also on the interfacial profile, which, in turn, depends on the size and shape of the inclusion (as specified by x_A, $\bar{s}_A$, and θ_A).

The solutions of the coexistence equations reveal that $n^B \gg n^H$, i.e., the transition takes place between a peptide-dilute L_α and a peptide-rich H_{II} phase. Moreover, from the two cases shown in Fig. 11, as well as calculations performed for several other systems (see below), it follows that whenever a transition takes place, the number of lipids per inclusion in the H_{II} phase, n^H, is quite insensitive to variations in either the inclusion or the lipid characteristics. This behavior is a direct consequence of the fact that whereas F^B varies only moderately with n^B (at the relevant range), F^H exhibits a pronounced minimum at $n^H = \hat{n}^H$. Thus the common tangent construction implies that $\hat{n}^H$ will also be the lipid content of the hexagonal phase at coexistence. Furthermore, $\hat{n}^H$ is mainly dictated by geometric packing constraints in the H_{II} phase. To better understand this argument, recall that in the inclusion-free H_{II} phase, some of the lipid chains are inevitably "frustrated." If the chains bridging water tubes are relaxed ($b \approx b_0$), the ones pointing toward the interstitial axes are strongly stretched, whereas if the latter are relaxed, the former are overcompressed (see Figs. 5 and 10). Neither long nor short (two-ended) inclusions can amend the former situation. On the other hand, short hydrophobic inclusions (with two hydrophilic anchor-

FIGURE 11 The free energy per inclusion in the hexagonal phase, $F^H = F_{el}^H$, and the bilayer phase, $F^B = F_{el}^B + F_{mix}^B$, as a function of the number of lipids per inclusion, n. Also shown is the elastic contribution to the bilayer free energy, F_{el}^B. The dotted lines describe the "common tangent" construction, and the coexistence values of n^B and n^H, as obtained by numerical solution of Eq. 23. The results shown correspond to a lipid system with $B = 320k_B T$ Å^2, containing inclusions characterized by $\bar{s}_A = -0.35$, $\theta_A = 0$ (*left*), and $\bar{s}_A = -0.30$, $\theta_A = 0.1$ (*right*).
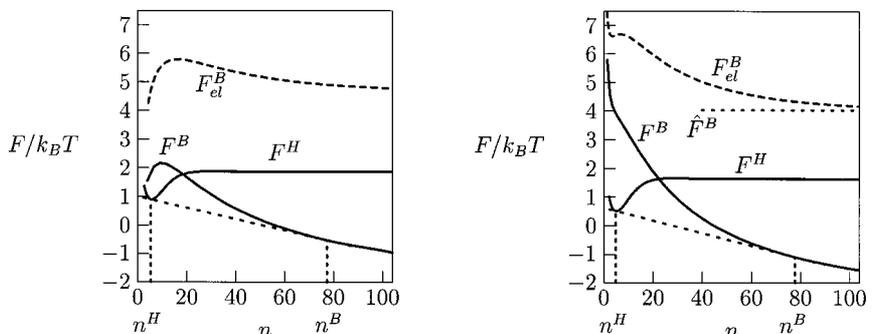
ing ends) can remedy the latter case by replacing the over-compressed chains. This also implies that just a small and geometrically well-defined number of chains ($\hat{n}^H$ per inclusion), all with $b \approx b_0$, are required to fill up the rest of the hydrophobic domain. Depending on the details of the inclusion shape, we find $\hat{n}^H \approx 5\text{--}10$. The experimentally measured value, for short α-helical peptides, is $n^H \approx 6$ (Killian et al., 1996). The extent to which and the direction in which (barrel-like or vase-like) these peptides deviate from the straight-cylindrical shape are not entirely obvious.

The moderate variation of $F^B(n^B)$ in the inclusion-dilute (large n^B) regime is mainly due to the mixing term, F_{mix} (n^B). The elastic free energy, $F_{el}^B(n^B)$, is nearly constant there and given, approximately, by the elastic deformation energy of an isolated inclusion, $F_{el}^B = \hat{F}_{el}^B$. In the Theory section we have used this approximation, along with $F^H = \hat{F}^H = F^H (\hat{n}^H)$, to replace the two (exact) coexistence conditions (Eq. 23) with the single condition (Eq. 27). To test this approximation, we have used Eq. 27 to derive the coexistence characteristics of the same system already shown in Fig. 11. The results are shown in Fig. 12, revealing that the approximation is quite reasonable. More importantly, they confirm our interpretation that the $L_\alpha \rightarrow H_{II}$ transition is driven by the interplay between the mixing entropy of inclusions in the lamellar phase and the elastic energy difference between the two phases.

In Fig. 13 we collect the results of a systematic analysis, demonstrating the role of inclusion geometry and lipid elasticity in promoting the $L_\alpha \rightarrow H_{II}$ transition. As the "control parameter" we use the hydrophobic mismatch, $\bar{s}_A$. Four types of systems are considered, corresponding to different choices of inclusion shape and lipid spontaneous curvature. For each of these systems a pair of (either solid or dashed) curves shows how $1/n^B$ (*left*) and $1/n^H$ (*right*), the inclusion/lipid mole fraction ratio in the two coexisting phases, vary with $\bar{s}_A$. The solid curves were calculated using the simplified coexistence condition (Eq. 27). The dashed curves, shown for three of the four cases considered, were calculated using the full common tangent construction (Eq. 23). Cases a, b, and c correspond, respectively, to cylindri-

FIGURE 13   The number of inclusions per lipid $1/n^B$ and $1/n^H$, at coexistence, for different values of the mismatch $\bar{s}_A$. The two solid curves *a* show $1/n^B$ (*left*) and $1/n^H$ (*right*) for $B = 320k_BT$ Å^2 and $\theta_A = 0$. Changing the inclusion shape, we obtain curves *b* for a barrel-like inclusion ($\theta_A = 0.1$) and curves *c* for a vase-like inclusion ($\theta_A = -0.1$). Increasing the headgroup parameter to $B = 413k_BT$ Å^2 ($c_0 = 0$) at $\theta_A = 0$ leads to curves *d*. Solid lines refer to the solution of Eq. 27. For cases *a*, *b*, and *d* we also show the solution of the full "common tangent" equations, Eq. 23 (*broken lines*).

cal ($\theta_A = 0$), barrel-like ($\theta_A = 0.1$), and vase-like ($\theta_A = -0.1$) inclusions, all for lipids with $B = 320k_BT$ Å^2 ($c_0 \approx -(1/100)$Å^{-1}). In case d the inclusions are cylindrical and the lipid spontaneous curvature is $c_0 = 0$ ($B = 413k_BT$ Å^2).

One qualitative conclusion from the results in Fig. 13 is that a large negative hydrophobic mismatch is a necessary condition for the appearance of the bilayer–inverse-hexagonal phase transition. (The bottom ends of the curves mark the smallest value of $\bar{s}_A$ allowing the common tangent construction.) Quantitatively, the coexistence characteristics are also affected by the lipid spontaneous curvature and the inclusion shape. Large negative spontaneous curvatures and barrel-shaped inclusions facilitate the formation of the hexagonal phase. The difference between vase-like and cylindrical inclusions is very small.

Earlier in this section it was noted that the morphological transformation from the bilayer to the inverse-hexagonal structure is driven by the gain in elastic deformation energy, which is lower in the inclusion-containing hexagonal phase. This driving force is opposed by the loss of inclusion-lipid mixing entropy, which, according to our model, was assumed to be ideal (hence at maximum) in the bilayer phase and zero in the (ordered) hexagonal phase. Consequently, our estimates of $1/n^B$, the saturation inclusion content in the bilayer phase, may be regarded as an upper bound to the real value of this quantity. Another, rather extreme but theoretically interesting limit corresponds to the case where the inclusions are immobile not only in the hexagonal phase, but also in the bilayer. In this case one expects the $L_\alpha \rightarrow H_{II}$ transition to appear at lower values of n_B. Furthermore, the minimum values of $|\bar{s}_A|$ necessary to induce the transition should be smaller than our previous estimates. Both of these expectations were corroborated by detailed calculations (based on "freezing" the bilayer inclusions in ordered ar-

FIGURE 12   Free energy per inclusion in the hexagonal phase, F^H, and in the bilayer phase, F^B, as a function of the number of lipids per inclusion, n. Here, the elastic bilayer free energy, F_{el}^B, is approximated by $\hat{F}_{el}^B$ (*broken line*). The values of n^B and n^H at coexistence are derived using Eq. 27. The system is the same as in the left diagram of Fig. 11 ($B = 320k_BT$ Å^2, $\bar{s}_A = -0.35$, and $\theta_A = 0$).

rays). We found, for example, that for a system of perfectly cylindrical inclusions embedded in lipid bilayers with $B = 320k_BT$ Å^2, the threshold value of the hydrophobic mismatch is lowered from $\bar{s}_A = -0.32$ (see Fig. 13) to $\bar{s}_A \approx -0.20$.

CONCLUDING REMARKS

We had two major goals in this paper. One quite general goal was to present a new model for lipid-protein interaction, based on a molecular-level representation of the principal forces governing lipid self-assembly, namely, headgroup repulsion, tail repulsion, and the hydrocarbon-water surface energy. This molecular scheme, although approximate, can account for many important characteristics of lipid organization, including detailed structural information, such as the extent of faceting in the inverse hexagonal phase. One significant feature of our molecular model involves the explicit inclusion of two variational degrees of freedom: the chain length and the chain tilt angle. This has enabled us to evaluate the elastic deformation energy associated with the presence of differently shaped hydrophobic inclusions, in both the bilayer and inverse-hexagonal phases. The molecular constants appearing in the basic expression for the molecular free energy can be estimated by using known structural information or on the basis of more detailed theoretical calculations. More significantly, these molecular constants are intimately related to the elastic characteristics of the lipid layer.

After presenting the molecular model and describing how to use it for calculating the lipid-mediated interaction between inclusions, the model has been employed to calculate the inclusion-induced deformation energies of the bilayer and inverse-hexagonal phases. It was then straightforward to apply the model to the study of the inclusion-induced $L_\alpha \rightarrow H_{II}$ transition. This has been the second major goal of this paper. Our analysis was motivated by systematic experimental studies demonstrating the ability of some synthetic helical peptides and gramicidin A proteins to promote this transition in systems which, in the absence of these inclusions, form stable bilayers (Killian et al., 1996; Morein et al., 1997). In agreement with these experiments, we found that only short ("negative mismatch") peptides can drive the $L_\alpha \rightarrow H_{II}$ transition. Consistent with experiment, we also found that, at coexistence, the peptide content in the hexagonal phase is much larger than in the lamellar phase.

Some predictions of the model still await experimental verification. For example, our conclusion that the degree of hydrophobic mismatch necessary to induce the $L_\alpha \rightarrow H_{II}$ transition may be reduced by choosing lipids of large negative spontaneous curvature. Similarly, it remains to be seen whether barrel-like proteins are, indeed, more effective promoters of the transition than vase-like or cylinder-like proteins. Finally, it should be mentioned that we have not considered here the possibility that the $L_\alpha \rightarrow H_{II}$ transition will be preempted by other phase transitions, primarily two-dimensional phase separation phenomena.

APPENDIX A: MONOLAYER AREA AND VOLUME ELEMENTS

Consider a symmetrical lipid bilayer. Its symmetry implies that its midplane is perfectly flat. We describe the hydrocarbon-water surface of, say, the external monolayer by the local chain length, $b(r)$, and tilt angle, $\theta(r)$. Both functions are assumed to depend only on the distance, r, from the inclusion midaxis. Our aim is to determine the functions $g_A(r)$ and $g_V(r)$ appearing, respectively, in our expressions for the interfacial area and hydrophobic volume, $dA = d\psi\, dr\, rg_A(r)$ and $dV = d\psi\, dr\, rg_V(r)$, as introduced after Eqs. 13 and 14. Note that dA and dV are determined by $b(r)$, $\theta(r)$, $b(r + dr)$, and $\theta(r + dr)$ as schematically shown in Fig. 14.

Defining $b_1 = b(r) \cos \theta(r)$, $r_1 = r - b(r) \sin \theta(r)$, $b_2 = b(r + dr) \cos \theta(r + dr)$, and $r_2 = r + dr - b(r + dr) \sin \theta(r + dr)$, we can write

$$dV = dV_C(r_1, r_2, b_1) + \tfrac{1}{2} dV_C(r_1, r_2, b_2 - b_1)$$

$$+ \tfrac{1}{2} dV_C(r_2, r + dr, b_2) - \tfrac{1}{2} dV_C(r_1, r, b_1)$$

$$dA = \sqrt{(b_2 - b_1)^2 + (r_2 - r_1)^2}\, \frac{r_1 + r_2}{2}\, d\phi$$

where the function

$$dV_C(r_1, r_2, h) = \frac{h}{2}(r_2^2 - r_1^2) d\phi$$

evaluates the volume of a rectangle of width $r_2 - r_1$ and height h that rotates around the small angle $d\psi$. Expanding dV and dA to first order in dr leads to

$$g_V(r) = b \cos \theta - \frac{b^2}{2}\theta' + \frac{b^3 \theta'}{2r} \sin \theta \left(1 - \frac{1}{2}\sin^2\theta\right)$$

$$- \frac{b^2}{2r}\sin \theta \cos \theta \left(1 - \frac{b'}{2}\sin \theta\right)$$

$$g_A(r) = \left(1 - \frac{b}{r}\sin \theta\right)$$

$$\sqrt{1 + b'^2 + b^2\theta'^2 - 2(b'\sin\theta + b\theta'\cos\theta)} \quad (28)$$

where the prime denotes the derivative with respect to r. The 1D versions of these functions, $g_V(x)$ and $g_A(x)$, are obtained from Eq. 28 by taking the limit $r = x \rightarrow \infty$.
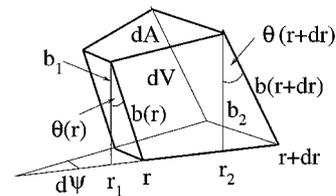
FIGURE 14   The local packing properties of the monolayer are characterized by the chain length, b, and tilt angle, θ, at the positions r and $r + dr$. They determine the interfacial area, dA, and hydrophobic volume, dV.

REFERENCES

Aranda-Espinoza, H., A. Berman, N. Dan, P. Pincus, and S. A. Safran. 1996. Interaction between inclusions embedded in membranes. *Biophys. J.* 71:648–656.

Ben-Shaul, A. 1995. Molecular theory of chain packing, elasticity and lipid protein interaction in lipid bilayers. *In* Structure and Dynamics of Membranes, Vol. 1, 2nd Ed. R. Lipowsky and E. Sackmann, editors. Elsevier, Amsterdam. 359–402.

Chen, L., D. Bassolino, and T. Stouch. 1997. Transmembrane helix structure, dynamics, and interactions: multi-nanosecond molecular dynamics simulation. *Biophys. J.* 73:3–20.

Dan, N., A. Berman, P. Pincus, and S. A. Safran. 1994. Membrane-induced interactions between inclusions. *J. Phys. II France.* 4:1713–1725.

Dan, N., P. Pincus, and S. A. Safran. 1993. Membrane-induced interactions between inclusions. *Langmuir.* 9:2768–2771.

deGennes, P. G. 1979. Scaling Concepts in Polymer Physics. Cornell University Press, Ithaca, NY.

Dumas, F., M. M. Sperotto, M. C. Lebrun, J. F. Tocanne, and O. G. Mouritsen. 1997. Molecular sorting of lipids by bacteriorhodopsin in dilauroylphosphatidylcholine/distearoylphosphatidylcholine lipid bilayers. *Biophys. J.* 73:1940–1953.

Fattal, D. R., and A. Ben-Shaul. 1993. A molecular model for lipid protein interaction in membranes: the role of hydrophobic mismatch. *Biophys. J.* 65:1795–1809.

Gelbart, W. M., and A. Ben-Shaul. 1987. Chain packing and the compressional elasticity of surfactant films. *In* Springer Proceedings in Physics, Vol. 21: Physics of Amphiphilic Layers. J. Meunier, D. Langevin and N. Boccara, editors. Springer Verlag, Berlin. 9–12.

Goulian, M., R. Bruinsma, and P. Pincus. 1993. Long-range forces in heterogeneous fluid membranes. *Europhys. Lett.* 22:145–150.

Guggenheim, E. A. 1949. *Thermodynamics.* North-Holland, Amsterdam.

Hamm, M., and M. M. Kozlov. 1998. Tilt model of inverted amphiphilic mesophases. *Europhys. B.* (in press).

Helfrich, P., and E. Jakobsson. 1990. Calculation of deformation energies and conformations in lipid membranes containing gramicidin channels. *Biophys. J.* 57:1075–1084.

Helfrich, W. 1973. Elastic properties of lipid bilayers: theory and possible experiments. *Z. Naturforsch.* 28:693–703.

Huang, H. W. 1986. Deformation free energy of bilayer membrane and its effect on gramicidin channel lifetime. *Biophys. J.* 50:1061–1070.

Israelachvili, J. N. 1992. *Intermolecular and Surface Forces,* 2nd Ed. Academic Press, San Diego.

Killian, J. A. 1992. Gramicidin and gramicidin-lipid interactions. *Biophys. Biochim. Acta.* 1113:391–425.

Killian, J. A. 1998. Hydrophobic mismatch between proteins and lipids in membranes. *Biophys. Biochim. Acta.* (in press).

Killian, J. A., and B. deKruijff. 1988. Proposed mechanism for H_{II} phase induction by gramicidin in model membranes and its relation to channel formation. *Biophys. J.* 53:111–117.

Killian, J. A., I. Salemink, M. R. R. dePlanque, G. Lindblom, R. E. Koeppe, and D. V. Greathouse. 1996. Indication of nonbilayer structures in diacylphosphatidylcholine model membranes by transmembrane α-helical peptides: importance of hydrophobic mismatch and proposed role of tryptophans. *Biochemistry.* 35:1037–1045.

Lewis, B. A., and D. M. Engelmann. 1983. Bacteriorhodopsin remains dispersed in fluid phospholipid bilayers over a wide range of bilayer thicknesses. *J. Mol. Biol.* 166:203–210.

Marcelja, S. 1976. Lipid-mediated protein interactions in membranes. *Biophys. Biochim. Acta.* 455:1–7.

Marsh, D. 1995. Lipid-protein interactions and heterogeneous lipid distribution in membranes. *Mol. Membr. Biol.* 12:59–64.

May, S., and A. Ben-Shaul. 1995. Spontaneous curvature and thermodynamic stability of mixed amphiphilic layers. *J. Chem. Phys.* 103: 3839–3848.

Morein, S., E. Strandberg, J. A. Killian, S. Persson, G. Arvidson, R. E. Koeppe, and G. Lindblom. 1997. Influence of membrane spanning α-helical peptides on the phase behavior of the dioleoylphosphatidylcholine/water system. *Biophys. J.* 73:3078–3088.

Mouritsen, O. G., and M. Bloom. 1984. Mattress model of lipid protein interactions in membranes. *Biophys. J.* 46:141–153.

Nielsen, C., M. Goulian, and O. S. Andersen. 1998. Energetics of inclusion-induced bilayer deformations. *Biophys. J.* 74:1966–1983.

Piknova, B., E. Perochon, and J. F. Tocanne. 1993. Hydrophobic mismatch and long-range protein/lipid interactions in bacteriorhodopsin/phosphatidylcholine vesicles. *Eur. J. Biochem.* 218:385–396.

Ren, J., S. Lew, Z. Wang, and E. London. 1997. Transmembrane orientation of hydrophobic α-helices is regulated both by the relationship of helix length to bilayer thickness and by the cholesterol concentration. *Biochemistry.* 36:10213–10220.

Ryba, N. J. P., and D. Marsh. 1992. Protein rotational diffusion and lipid/protein interactions in recombinants of bovine rhodopsin with saturated diacylphosphatidylcholines of different chain lengths studied by conventional and saturation-transfer electron spin resonance. *Biochemistry.* 31:7511–7518.

Seddon, J. M. 1990. Structure of the inverted hexagonal (H_{II}) phase, and non-lamellar phase transitions of lipids. *Biophys. Biochim. Acta.* 1031: 1–69.

Siegel, D. P., and R. M. Epand. 1997. The mechanism of lamellar-to-inverted hexagonal phase transitions in phosphatidylethanolamine: implications for membrane fusion mechanisms. *Biophys. J.* 73:3089–3111.

Sperotto, M. M. 1997. A theoretical model for the association of amphiphilic transmembrane peptides in lipid bilayers. *Eur. Biophys. J.* 26: 405–416.

Tanford, C. 1980. *The Hydrophobic Effect,* 2nd Ed. Wiley Interscience, New York.

Turner, D. C., and S. M. Gruner. 1992. X-ray diffraction reconstitution of the inverted hexagonal (H_{II}) phase in lipid-water systems. *Biochemistry.* 31:1340–1355.